Available online at www.sciencedirect.com

SCIENCE DIRECT®

ELSEVIER

International Journal of Machine Tools & Manufacture 46 (2006) 1489–1499

INTERNATIONAL JOURNAL OF MACHINE TOOLS & MANUFACTURE DESIGN, RESEARCH AND APPLICATION

www.elsevier.com/locate/ijmactool

Analytical models for high performance milling. Part II: Process dynamics and stability

E. Budak*

Faculty of Engineering and Natural Sciences, Sabanci University, Istanbul, Turkey

Received 15 July 2005; received in revised form 17 September 2005; accepted 22 September 2005
Available online 10 November 2005

Abstract

Chatter is one of the most important limitations on the productivity of milling process. In order to avoid the poor surface quality and potential machine damage due to chatter, the material removal rate is usually reduced. The analysis and modeling of chatter is complicated due to the time varying dynamics of milling chatter which can be avoided without sacrificing the productivity by using analytical methods presented in this paper.

1. Introduction

Productivity and surface quality in milling processes have direct effects on cost, production lead-time and quality of machined parts. Chatter is one of the most common limitations for productivity and part quality in milling operations. Poor surface finish with reduced productivity and decreased tool life are the usual results of chatter. Additional operations, mostly manual, are required to clean the chatter marks left on the surface. Thus, chatter vibrations result in reduced productivity, increased cost and inconsistent product quality. The importance of modeling and predicting stability in milling has further increased within last couple of decades due to the advances in high speed milling technology. At high speeds, the stabilizing effect of process damping diminishes making process more prone to chatter. On the other hand, high stability limits, usually referred to as stability lobes, exist at certain high spindle speeds which can be used to increase chatter-free material removal rate substantially provided that they are predicted accurately.

Chatter vibrations develop due to dynamic interactions between the cutting tool and workpiece. Under certain conditions the amplitude of vibrations grows and the cutting system becomes unstable. Although chatter is always associated with vibrations, in fact it is fundamentally due to instability in the cutting system. The first accurate modeling of self-excited vibrations in orthogonal cutting was performed by Tlusty [1] and Tobias [2]. They identified the most powerful source of self-excitation, *regeneration*, which is associated with the dynamics of the machine tool and the feedback between the subsequent cuts on the same cutting surface. The stability analysis of milling is complicated due to the rotating tool, multiple cutting teeth, periodical cutting forces and chip-load directions, and multi-degree-of-freedom structural dynamics. In the early milling stability analysis, Koenigsberger and Tlusty [3] used the orthogonal chatter model [1] considering an average direction and average number of teeth in cut. An improved approximation was performed by Opitz et al. [4]. Sridhar et al. [5,6] performed a comprehensive analysis of milling stability which involved numerical evaluation of the dynamic milling system's state transition matrix. On a two-degree-of-freedom cutter model with point contact, Minis et al. [7] used Floquet's theorem and the Fourier series for the formulation of the milling stability, and numerically solved it using the Nyquist criterion. Budak [8] developed a stability method which leads to analytical determination of stability limits in milling. The method was verified by experimental and numerical results [9,10], applied to the stability of ball-end milling [11], and was also extended to 3D milling [12]. The special case of low immersion milling has been investigated

*Tel.: +902164839519; fax: +902164839550.
E-mail address: ebudak@sabanciuniv.edu.

0890-6955/$ - see front matter © 2005 Elsevier Ltd. All rights reserved.
doi:10.1016/j.ijmachtools.2005.09.010

in several studies where added lobes were also presented [13–15]. Recently, Merdol and Altintas [16] demonstrated that the original multi-frequency stability model of Budak and Altintas [8–10] can also be used to predict the added lobes in case of very low immersion milling.

Another method of chatter suppression in milling is the application of cutting tools with irregular spacing, or *variable pitch cutters* which are particularly useful in cases where high stability lobes cannot be utilized due to speed limitations for the machine or work material. Unlike the stability lobe or process damping effects, they can be effective for both high- and low-speed applications. The effectiveness of variable pitch cutters in suppressing chatter was first demonstrated by Slavicek [17] by assuming a rectilinear motion. Opitz et al. [18] considered milling tool rotation using average directional factors. Another significant study on these cutters was performed by Vanherck [19] who considered different pitch variation patterns in the analysis but by assuming rectilinear tool motion. Later, Tlusty et al. [20] analyzed the stability of milling cutters with special geometries such as irregular pitch or serrated edges, using numerical simulations. Their results confirmed that for a certain pitch variation, high improvements in stability can be achieved only for a limited speed and chatter frequency ranges. Altintas et. al. [21] adapted the analytical milling stability model to the case of variable pitch cutters which can be used to predict the stability limits accurately. Recently, Budak [22] developed an analytical method for the optimal design of pitch angles in order to maximize stability limit for chatter frequency and spindle speed ranges of interest.

One important input needed by the chatter models is the dynamic properties of the milling system which are usually measured using impact testing and modal analysis [23]. Considering great variety of machine tool configurations, tool holder and cutting tool geometries, analysis of every case can be quite time consuming and unpractical. Schmitz [24,25] used substructuring methods to predict the dynamics of tool holder-end mill assembly using beam component modes. Kivanc and Budak [26] further extended this approach by including the complex geometry of end mills in the beam model.

In this paper, methods of increasing chatter-free material rate by optimal selection of tool geometry, spindle speed and axial and radial depth of cuts are presented. The methodology is mainly based on the original analytical milling stability model of Budak and Altintas [8–10]. A practical method for tool dynamics modelling is also given.

2. Stability analysis of standard milling tools

2.1. Dynamic chip thickness and milling forces

In this analysis, both milling cutter and work piece are considered to have two orthogonal modal directions as shown in Fig. 1. Milling forces excite both cutter and workpiece causing vibrations which are imprinted on the cutting surface. Each vibrating cutting tooth removes the wavy surface left from the previous tooth resulting in modulated chip thickness which can be expressed as follows:

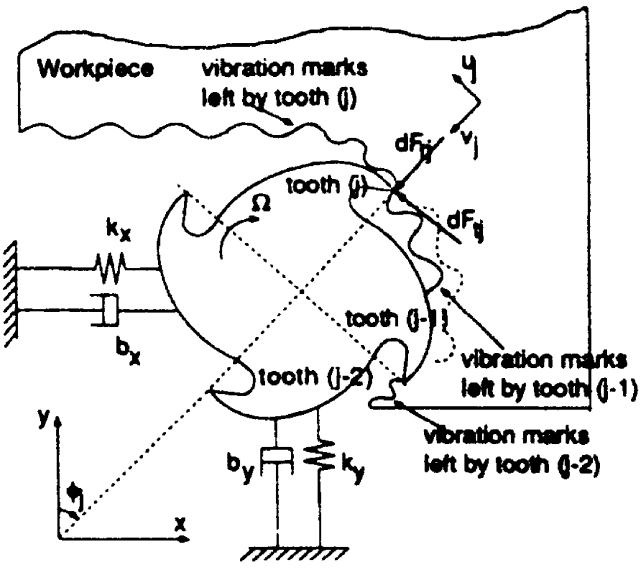

Fig. 1. Cross sectional view of an end mill showing differential forces.

$$h_j(\phi) = f_t \sin \phi_j + \left(v_{j_c}^0 - v_{j_w}^0\right) - \left(v_{j_c} - v_{j_w}\right), \tag{1}$$

where the feed per tooth f_t represents the static part of the chip thickness, and $\phi_j = (j-1)\phi_p + \phi$ is the angular immersion of tooth (j) for a cutter with constant pitch angle $\phi_p = 2\pi/N$ and N teeth as shown in Fig. 1. $\phi = \Omega t$ is the angular position of the cutter measured with respect to the first tooth and corresponding to the rotational speed Ω (rad/sec). v_j and v_j^0 are the dynamic displacements in the chip thickness direction due to tool and work piece vibrations for the current and previous tooth passes, for the angular position ϕ_j, and can be expressed in terms of the fixed coordinate system as follows:

$$v_{j_p} = -x_p \sin \phi_j - y_p \cos \phi_j \quad (p = c, w), \tag{2}$$

where p and c indicate part and cutter, respectively.

The static part in Eq. (1), $(f_t \sin \phi_j)$, is neglected in the stability analysis, as it does not contribute to the regeneration mechanism, and thus can be eliminated in the chatter stability analysis.

If Eq. (2) is substituted in Eq. (1), the following expression is obtained for the dynamic chip thickness in milling:

$$h_j(\phi) = \left[\Delta x \sin \phi_j + \Delta y \cos \phi_j\right], \tag{3}$$

where

$$\begin{aligned} \Delta x &= \left(x_c - x_c^0\right) - \left(x_w - x_w^0\right), \\ \Delta y &= \left(y_c - y_c^0\right) - \left(y_w - y_w^0\right), \end{aligned} \tag{4}$$

where (x_c, y_c) and (x_w, y_w) are the dynamic displacements of the cutter and the work piece in the x and y directions, respectively. The dynamic cutting forces on tooth (j) in the tangential and the radial directions can be expressed as follows:

$$F_{t_j}(\phi) = K_t a h_j(\phi); F_{r_j}(\phi) = K_r F_{t_j}(\phi), \tag{5}$$

where a is the axial depth of cut, and K_t and K_r are the cutting force coefficients. After substituting h_j from equation, the dynamic milling forces can be resolved in x and y directions as follows:

$$\begin{Bmatrix} F_x \\ F_y \end{Bmatrix} = \frac{1}{2} a K_t \begin{bmatrix} a_{xx} & a_{xy} \\ a_{yx} & a_{yy} \end{bmatrix} \begin{Bmatrix} \Delta x \\ \Delta y \end{Bmatrix}, \tag{6}$$

where a_{xy} are the directional coefficients [9,10]. The directional coefficients depend on the angular position of the cutter which makes Eq. (6) time varying:

$$\{F(t)\} = \tfrac{1}{2} a K_t [A(t)]\{\Delta(t)\}. \tag{7}$$

$[A(t)]$ is periodic at the tooth passing frequency $\omega = N\Omega$. In general, the Fourier series expansion of the periodic term is used for the solution of the periodic systems. However, in chatter stability analysis the inclusion of the higher harmonics in the solution may not be required for most cases as the response at the chatter limit is usually dominated with a single chatter frequency. Starting from this idea, Budak and Altintas [8–10] and later Merdol and Altintas [16] have shown that the higher harmonics do not affect the accuracy of the predictions unless the radial depth of cut is extremely small compared to the tool diameter. Thus, it is sufficient to include only the average term in the Fourier series expansion of $[A(t)]$ in which case the directional coefficients take the following form [8–10]:

$$\begin{aligned} \alpha_{xx} &= \tfrac{1}{2}[\cos 2\phi - 2K_r\phi + K_r \sin 2\phi]_{\phi_{st}}^{\phi_{ex}}, \\ \alpha_{xy} &= \tfrac{1}{2}[-\sin 2\phi - 2\phi + K_r \cos 2\phi]_{\phi_{st}}^{\phi_{ex}}, \\ \alpha_{yx} &= \tfrac{1}{2}[-\sin 2\phi + 2\phi + K_r \cos 2\phi]_{\phi_{st}}^{\phi_{ex}}, \\ \alpha_{yy} &= \tfrac{1}{2}[-\cos 2\phi - 2K_r\phi - K_r \sin 2\phi]_{\phi_{st}}^{\phi_{ex}}. \end{aligned} \tag{8}$$

Then, Eq. (7) reduces to the following form:

$$\{F(t)\} = \tfrac{1}{2} a K_t [A_0]\{\Delta(t)\}. \tag{9}$$

2.2. Chatter stability limit

The dynamic displacement vector in Eq. (9) can be determined using the dynamic properties of the structures, transfer function or frequency response functions, and the dynamic forces. By substituting the response and the delay terms in Eq. (9), the following expression is obtained [9,10]:

$$\{\mathrm{F}\}e^{i\omega_c t} = \tfrac{1}{2} a K_t (1 - e^{-i\omega_c T})[A_0][G(i\omega_c)]\{\mathrm{F}\}e^{i\omega_c t}, \tag{10}$$

where $\{\mathrm{F}\}$ represents the amplitude of the dynamic milling force $\{F(t)\}$, and the transfer function matrix is given as:

$$[G_p] = \begin{bmatrix} G_{p_{xx}} & G_{p_{xy}} \\ G_{p_{yx}} & G_{p_{yy}} \end{bmatrix} \quad (p = c, w), \tag{11}$$

where the total transfer function can be obtained from the summation of the cutter and workpiece transfer function, i.e., $[G(i\omega_c)] = [G_c(i\omega_c)] + [G_w(i\omega_c)]$. Eq. (10) has a non-trivial solution only if its determinant is zero,

$$\det[[I] + \Lambda[G_0(i\omega_c)]] = 0, \tag{12}$$

where $[I]$ is the unit matrix, and the oriented transfer function matrix is defined as

$$[G_0] = [A_0][G] \tag{13}$$

and the eigenvalue (Λ) in Eq. (12) is given as

$$\Lambda = -\frac{N}{4\pi} K_t a (1 - e^{-i\omega_c T}). \tag{14}$$

Λ can easily be computed from Eq. (12) numerically. However, an analytical solution is possible if the cross transfer functions, G_{xy} and G_{yx}, are neglected:

$$\Lambda = -\frac{1}{2a_0}\left(a_1 \pm \sqrt{a_1^2 - 4a_0}\right), \tag{15}$$

where

$$\begin{aligned} a_0 &= G_{xx}(i\omega_c) G_{yy}(i\omega_c)(\alpha_{xx}\alpha_{yy} - \alpha_{xy}\alpha_{yx}), \\ a_1 &= \alpha_{xx} G_{xx}(i\omega_c) + \alpha_{yy} G_{yy}(i\omega_c). \end{aligned} \tag{16}$$

Since the transfer functions are complex, Λ will have complex and real parts. However, the axial depth of cut (a) is a real number. Therefore, when $\Lambda = \Lambda_R + i\Lambda_I$ and $e^{-i\omega_c T} = \cos\omega_c T - i \sin\omega_c T$ is substituted in Eq. (14), the complex part of the equation has to vanish yielding

$$\kappa = \frac{\Lambda_I}{\Lambda_R} = \frac{\sin\omega_c T}{1 - \cos\omega_c T}. \tag{17}$$

The above can be solved to obtain a relation between the chatter frequency and the spindle speed [9,10]:

$$\begin{aligned} \omega_c T &= \varepsilon + 2k\pi, \\ \varepsilon &= \pi - 2\psi, \\ \psi &= \tan^{-1}\kappa, \\ n &= \frac{60}{NT}, \end{aligned} \tag{18}$$

where ε is the phase difference between the inner and outer modulations, k is an integer corresponding to the number of vibration waves within a tooth period, and n is the spindle speed (rpm). After the imaginary part in Eq. (14) is vanished, the following is obtained for the stability limit:

$$a_{lim} = -\frac{2\pi\Lambda_R}{NK_t}(1 + \kappa^2). \tag{19}$$

Therefore, for given cutting geometry, cutting force coefficients, tool and work piece transfer functions, and chatter frequency ω_c, Λ_I and Λ_R can be determined from Eq. (15), and can be used in Eqs. (18) and (19) to determine the corresponding spindle speed and stability limit. Eq. (15)

provides two Λ's for every chatter frequency, however the one which results in the lowest $a_{\lim}$ must be used similar to the other stability problems. When this procedure is repeated for a range of chatter frequencies and number of vibration waves, k, the stability lobe diagram for a milling system is obtained. Stability diagrams can be used to determine the maximum chatter free cutting depths and spindle speeds, and hence can be used to maximize the productivity without sacrificing from the quality.

3. Stability analysis for variable pitch cutters

3.1. Phase angles and stability limit

Variable pitch cutters have non-uniform pitch spacing between the cutting teeth. Thus, the fundamental difference in the stability analysis is that the phase delay is different for each tooth:

$$\varepsilon_j = \omega_c T_j \quad (j = 1, \ldots, N), \tag{20}$$

where T_j is the jth tooth period corresponding to the pitch angle ϕ_{pj}. The dynamic chip thickness and the cutting force relations given for the standard milling cutters apply to the variable pitch cutters, as well. The eigenvalue expression will take the following form due to the varying phase:

$$\Lambda = \frac{a}{4\pi} K_t \sum_{j=1}^{N} \left(1 - e^{-i\omega_c T_j}\right), \tag{21}$$

The stability limit can be obtained from Eq. (21) as

$$a_{\lim}^{vp} = -\frac{4\pi}{K_t} \frac{\Lambda}{N - C + iS}, \tag{22}$$

where

$$C = \sum_{j=1}^{N} \cos \omega_c T_j, \quad S = \sum_{j=1}^{N} \sin \omega_c T_j. \tag{23}$$

As $a_{\lim}$ is a real number, the imaginary part of Eq. (22) must vanish yielding [22]

$$a_{\lim}^{vp} = -\frac{4\pi}{K_t} \frac{\Lambda_I}{S}. \tag{24}$$

The stability limit with variable pitch cutters can be determined using Eq. (24). However, optimization of pitch angles for a given milling system has more practical importance than the stability analysis for an arbitrary variable pitch cutter. Therefore, the rest of the analysis focuses on the optimization of the pitch angles to maximize the stability against chatter.

Eq. (24) indicates that in order to maximize the stability limit, $|S|$ has to be minimized. From Eq. (23), S can be expressed as follows:

$$S = \sin \varepsilon_1 + \sin \varepsilon_2 + \sin \varepsilon_3 + \ldots, \tag{25}$$

where $\varepsilon_j = \omega_c T_j$. The phase angle, which is different for every tooth due to the non-constant pitch, can be expressed as follows:

$$\varepsilon_j = \varepsilon_1 + \Delta\varepsilon_j \ (j = 2, \ldots, N), \tag{26}$$

where $\Delta\varepsilon_j$ is the phase difference between tooth j and tooth (1) corresponding to the difference in the pitch angles between these teeth. The pitch angle variation ΔP corresponding to $\Delta\varepsilon$ can be determined as [22]

$$\Delta P = \frac{\Omega}{\omega_c} \Delta\varepsilon. \tag{27}$$

Eq. (25) can be expanded as follows by using Eq. (26):

$$S = \sin \varepsilon_1 + \sin \varepsilon_1 \cos \Delta\varepsilon_2 + \sin \Delta\varepsilon_2 \cos \varepsilon_1 + \sin \varepsilon_1 \cos \Delta\varepsilon_3 + \sin \Delta\varepsilon_3 \cos \varepsilon_1 + \ldots. \tag{28}$$

There are many solutions to the minimization of $|S|$, i.e. $(S = 0)$. For example, for even number of teeth, $S = 0$ for $\Delta\varepsilon_j = j\pi\cdot$ A more general solution can be obtained by substituting a specific pitch variation pattern into S. For the linear pitch variation S takes the following form [22]:

$$S = \sin \varepsilon_1 (1 + \cos \Delta\varepsilon + \cos 2\Delta\varepsilon + \ldots) + \cos \varepsilon_1 (\sin \Delta\varepsilon + \sin 2\Delta\varepsilon + \ldots). \tag{29}$$

It can be found out by intuition that $S = 0$ for the following conditions:

$$\Delta\varepsilon = k\frac{2\pi}{N} \quad (k = 1, 2, \ldots, N-1). \tag{30}$$

The corresponding ΔP can be determined using Eq. (27).

The increase of the stability with variable pitch cutters over the standard end mills can be determined by considering the ratio of stability limits. For simplicity, the absolute or critical stability limit for equal pitch cutters is used. The absolute stability limit is the minimum stable depth of cut without the effect of lobing which can be expressed as follows:

$$a_{cr} = -\frac{4\pi\Lambda_I}{N K_t}. \tag{31}$$

Then, the stability gain can be expressed as

$$r = \frac{a_{\lim}^{vp}}{a_{cr}} = \frac{N}{S}, \tag{32}$$

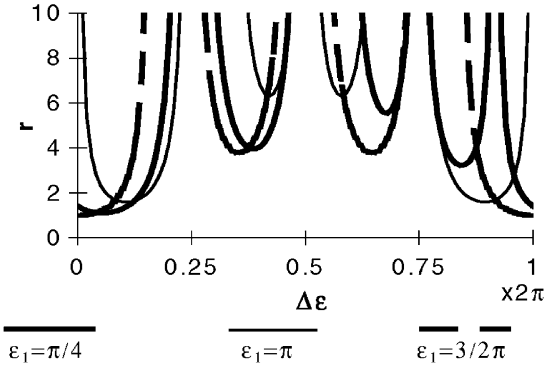

Fig. 2. Effect of ε_1 on stability gain for a 4-fluted end mill with linear pitch variation.

where r is plotted as a function of $\Delta\varepsilon$ in Fig. 2 for a 4-tooth milling cutter with linear pitch variation. The phase ε depends on the chatter frequency, spindle speed and the eigenvalue of the characteristic equation. Therefore, the stability analysis has to be performed for the given conditions. Three different curves corresponding to different ε_1 values are shown in Fig. 2 to demonstrate the effect of phase variation on r. r is maximized for integer multiples of $2\pi/N$, i.e. for $(1/4, 1/2, 3/4) \times 2\pi$. $\Delta\varepsilon + k2\pi (k = 1, 2, 3, \ldots)$ are also optimal solutions, however, they result in higher pitch variations which is not desired.

As it can be seen from Fig. 2 for a 4-tooth end mill with linear pitch variation, a minimum of $r = 4$ gain is obtained for $0.5\pi < \Delta\varepsilon < 1.5\pi$. Thus, the target for $\Delta\varepsilon$ should be π, which is one of the optimal solutions for the cutters with even number of flutes, but it is also in the middle of the high stability area.

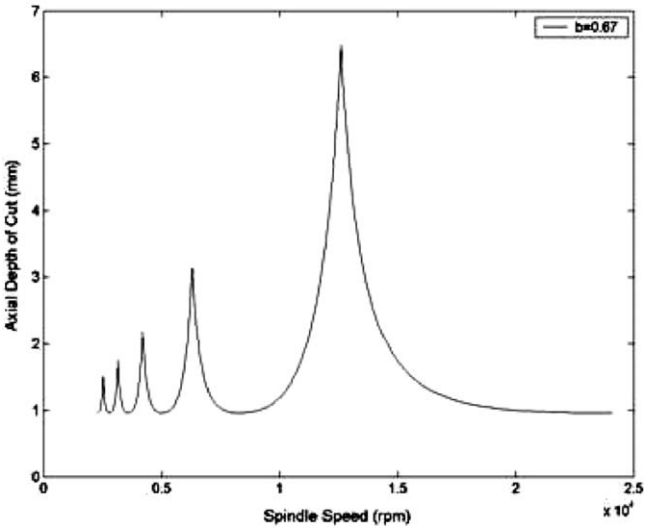

Fig. 3. Stable axial depth of cut vs. spindle speed for $b = 0.67$.

3.2. Design of milling cutters with linear pitch variation

Considering possible frequency variations, it is better to keep $\Delta\varepsilon$ close to π, i.e. $k = N/2$ for even number of teeth, $k = (N \pm 1)/2$ for odd number of teeth. Then, the relation between the pitch angle variation and the phase given in Eq. (27) takes the following form:

$$\begin{aligned} \Delta P &= \pi \tfrac{\Omega}{\omega_c} && \text{for even } N, \\ \Delta P &= \pi \tfrac{\Omega}{\omega_c} \tfrac{(N\pm1)}{N} && \text{for odd } N, \end{aligned} \tag{33}$$

where Ω is the spindle speed in (rad/s), $\Delta\varepsilon$ is the pitch variation (rad) and N is the number of teeth.

The pitch angles have to satisfy the following relation:

$$P_0 + (P_0 + \Delta P) + (P_0 + 2\Delta P) + \ldots\ldots + [P_0 + (N-1)\Delta P] = 2\pi. \tag{34}$$

P_0 can be determined from Eq. (34) as follows:

$$P_0 = \frac{2\pi}{N} - \frac{(N-1)\Delta P}{2}. \tag{35}$$

Therefore, for given chatter frequency and spindle speed, the optimal pitch variation can be determined from Eqs. (33) and (35).

4. Optimal conditions for stable milling using analytical models

4.1. Stable axial and radial depth of cuts

Stability diagrams in terms of axial depth of cut for a given radial depth of cut can be generated using Eq. (19) in a certain spindle speed range. The radial depth of cut, B, can be defined as follows:

$$\begin{aligned} B/R &= 1 - \cos(\phi_{st}) \quad \text{(up-milling)}, \\ B/R &= 1 + \cos(\phi_{ex}) \quad \text{(down-milling)}, \end{aligned} \tag{36}$$

where ϕ_{st} and ϕ_{ex} are the start and exit angles of the cutting edges to and from the cut, and R is the tool radius. A normalized form of the radial depth of cut, $b = B/2R$ is used in the rest of the formulation for generalization. Thus, b is unitless, and it may only have values in the range of [0, 1]. The stability diagrams can be generated, in terms of either a_{lim} vs. spindle speed (for a fixed b_{lim}) or b_{lim} vs. spindle speed (for a fixed a_{lim}). The common practice is to express stability diagrams in terms of a_{lim} vs. spindle speed. The importance of identifying b_{lim} is two folds. First, in some cases, axial depth is fixed due to the geometry of the part, thus the maximum stable b must be determined. Second, maximum MRR can only be achieved by optimizing both depth of cuts. The procedure to determine b_{lim} starts with selection of an a_{lim} for which the stability diagram, b_{lim} vs. spindle speed, will be generated. Then, by scanning the full range of exit angles (up-milling) or start angles (down-milling), the eigenvalues of the milling system are determined. As the last step, the corresponding value of b_{lim} is determined using Eq. (36).

As an example, the system considered by Weck et al. in [27] which involves milling of an aluminium alloy with a 3-tooth end mill is considered. Figs. 3 and 4 show the stability diagrams generated using the analytical method. One importance of identifying b_{lim} is clearly seen in Fig. 4. The radial depth of cut limit for the selected axial depth reaches to the maximum value of $b = 1$ at some speeds. That is another reason why the maximum material removal rate can only be achieved by optimizing a and b simultaneously.

If we focus on a specific spindle speed where stability limits are the highest, i.e. in the lobes, we see that, no decrease in b is necessary for some increase in a, however, after a certain point, a negatively sloped relation exists between the stable limits of axial and radial depths of cut as represented in Fig. 5.

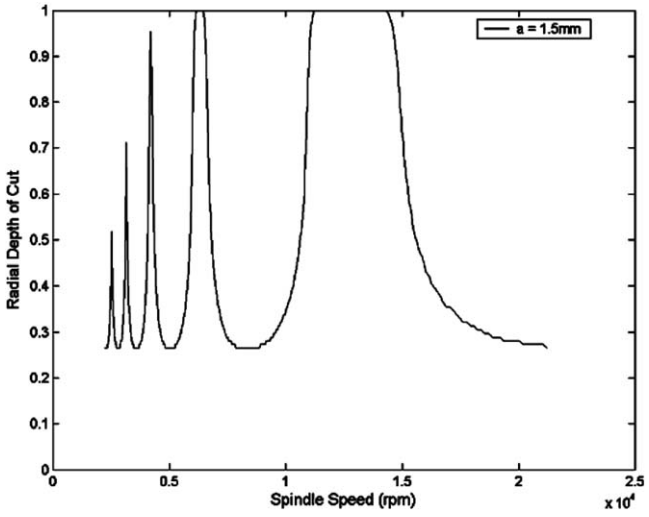

Fig. 4. Stable radial depth of cut vs. spindle speed for $a = 1.5$ mm.

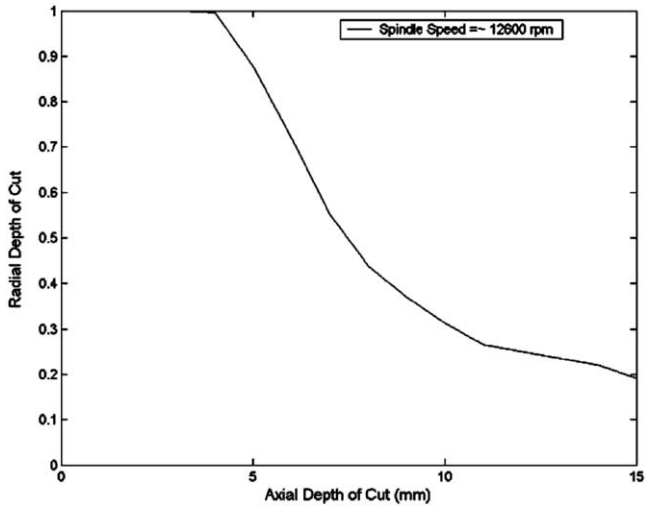

Fig. 5. Stable radial depth of cut vs. stable axial depth of cut for 12600 rpm.

4.2. Maximum material removal rate

Since material removal rate (MRR) is proportional to the multiplication of the axial and radial depths of cut, it is interesting to find out at which combination of axial and radial depths of cut, the maximum value of MRR may be achieved.

$$\mathrm{MRR} = a\,b\,n\,N\,f_t, \tag{37}$$

where, a is the axial depth of cut, b is the radial depth of cut, n is the spindle speed, N is the number of cutting teeth, and f_t is the feed per revolution per tooth. In general, effect of f_t on stability is small and can be neglected. Therefore, a normalized value of MRR is used hereafter:

$$\mathrm{MRR}^* = \frac{\mathrm{MRR}}{f_f} = a\,b\,n. \tag{38}$$

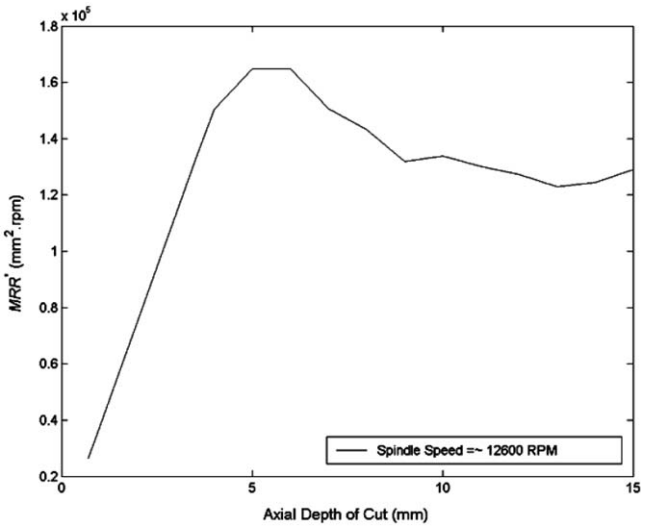

Fig. 6. Maximum MRR* vs. stable limit of axial depth of cut.

MRR* for an axial depth of cut is calculated using the b_{lim} corresponding to that a_{lim}. Subsequently the chatter-free MRR* is obtained as shown below:

$$\mathrm{MRR}^* = a_{\mathrm{lim}}\,b_{\mathrm{lim}}\,n\,N. \tag{39}$$

The variation of the MRR* with the axial depth of cut at the high stability pocket position of 12600 rpm is shown in Fig. 6. The figure indicates that, for this case, the maximum possible MRR* can be obtained for the axial depth of cut of about 5 mm. In some cases the MRR* curve has a peak as in Fig. 6, in some cases it saturates after a certain depth depending on the machine tool dynamics. Through simulations [28] it was found that if the natural frequencies of the cutter and workpiece system are different in x and y directions significantly, and the feed is in the direction of lower natural frequency, then it is more likely to see a peak in the MRR* curve. For the example considered here, the modal frequencies of the end mill in the feed and normal directions were 600 and 660 Hz, respectively.

4.3. Example applications

4.3.1. Stability limits

An aluminum milling application with 4-teeth milling tool is considered. The cutting coefficients were calibrated as $K_t = 796$ MPa and $K_r = 0.21$ for the feedrate of 0.25 mm/tooth. The modal properties of the tool measured using impact tests are given in [28]. The stability diagram in terms of radial depth for axial depth of cut of 1.5 mm is shown in Fig. 7. Results of the chatter tests are also shown in the same figure which are in good agreement with the predictions.

Fig. 8 shows the variation of the radial depth of cut limit with the axial depth for 11000 rpm which is useful in identifying the optimal milling conditions for maximum

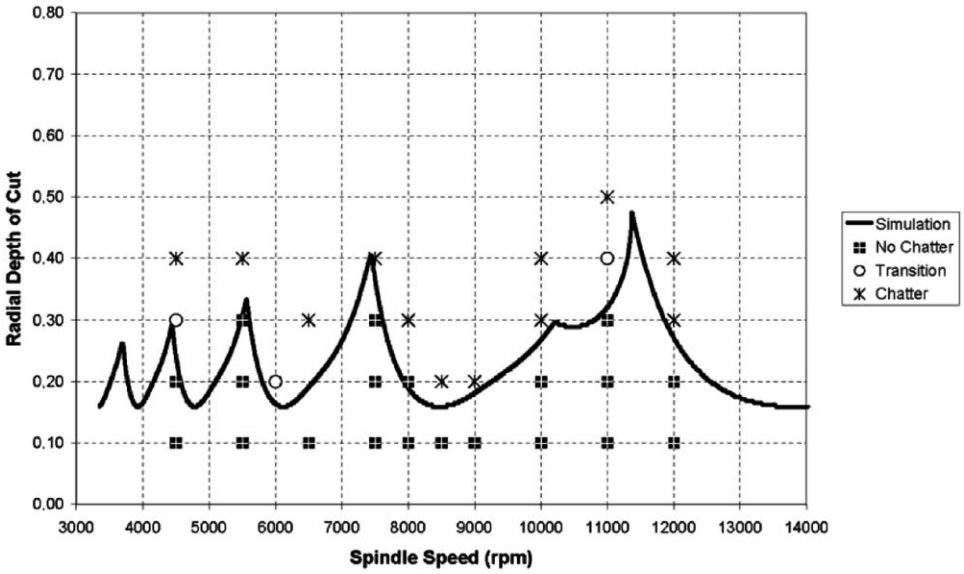

Fig. 7. Stability diagram for axial depth of 1.5 mm in the aluminum-milling example.

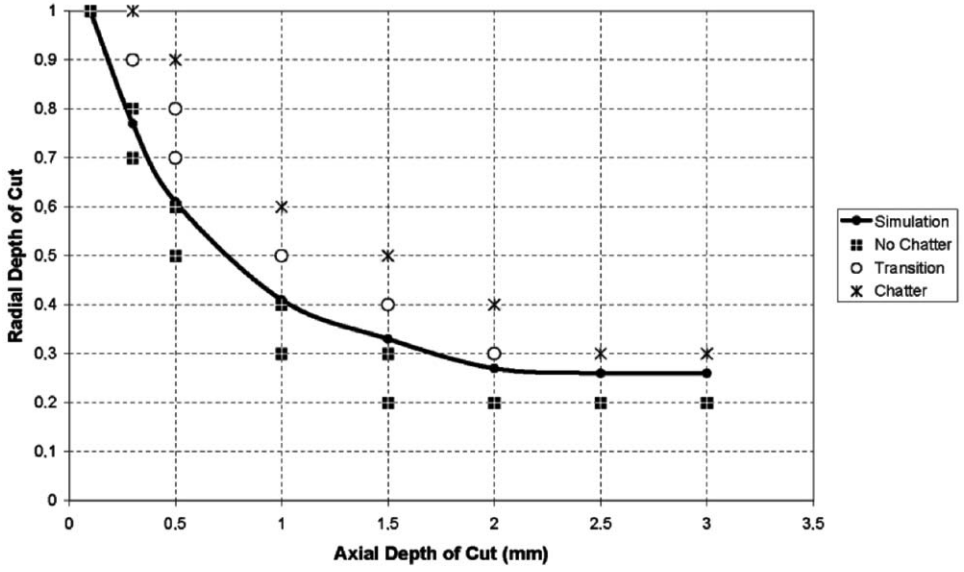

Fig. 8. Stable radial depth limit vs. axial depth of cut for 11 000 rpm.

material removal rate. Again, the agreement between experiments and the simulations is satisfactory.

4.3.2. Minimal chatter free pocketing time

Pocketing is a very common operation in milling, e.g. in die, mold, airframe production, etc. Pocketing time simply depends on the material removal rate and the dimensions of the pocket. In order to find the minimum pocketing time, one should consider the total number of passes (nop) [29]. The term "pass" stands for one cutting pass across the pocket length. Total pocketing time (TPT) can be approximately expressed as

$$\mathrm{TPT} = \mathrm{nop}\frac{w_p}{f}. \tag{40}$$

Thus, minimizing total pocketing time is equivalent to minimizing number of passes since we keep the feed rate constant throughout the analysis. A proper feedrate value should be used considering the other constraints such as the tool capacity and the surface finish requirement. Number of passes can then be expressed as

$$\mathrm{nop} = \mathrm{ceil}\left(\frac{d_\mathrm{p}}{a}\right)\mathrm{ceil}\left(\frac{l_\mathrm{p}}{b}\right), \tag{41}$$

Table 1
Pairs of stable limits of axial and radial depths of cut

a_{lim} (mm)	b_{lim} (mm)
4.00	1.00
6.00	0.83
8.00	0.65
10.00	0.52
12.00	0.44
14.00	0.38
20.00	0.27

Table 2
Optimal depths of cut for the minimum pocketing time

	Pocket	Conventional $b = 0.8$		Optimal			Improvement
D_p (mm)	L_p/D	a (mm)	nop	a (mm)	b	nop	(%)
4	10	4	13	4	1.0	13	23
6	10	6	13	6	0.83	13	8
8	10	4–4	26	8	0.65	16	38
10	10	5–5	26	10	0.52	20	23
12	10	6–6	26	12	0.44	23	11
14	10	5–5–4	39	14	0.38	27	30
20	10	5–5–5–5	52	20	0.27	38	27

where d_p is the pocket depth, l_p is the pocket length, ceil is the round up function. The ceil function is used, because even if the remaining part for the final pass is smaller than the geometry determined by axial and radial depths of cut, the time necessary for that final pass does not change. It is because of the ceil functions that maximizing MRR* is not necessarily same as minimizing nop. The steps of the proposed method are as follows. Once the pocket geometry and the appropriate tool are identified, workpiece and cutter dynamics are to be measured, so that the pairs of stable axial and radial depth of cut limits can be determined using simulations. For the example considered in Section 4.1, the pairs of stable depths are determined using the method presented here and shown in Table 1 [29]. Results of the optimization are presented in Table 2.

The first two column of Table 2 show the required pocket depth and length. The next two column-sets present the resulting nop for two different methods. The first method stands for choosing a high radial depth of cut close to full slotting, 0.8 in this case. The second column set, Optimal, presents the results for choosing the optimal pair of depths of cut according to the method presented in this paper. The last column shows the percentage improvements in pocketing time attained by the optimal combination.

Similar or even higher improvements in nop were obtained for other selected values of b. In conclusion, the optimal combination of axial and radial depths of cut, which gives the minimum pocketing time, might be quite different than those determined in by the conventional ways, i.e. arbitrarily picking a radial depth of cut. It is shown that by using the optimal combination, significant saving, up to around 40% reduction in pocketing time could be achieved.

5. Dynamic analysis of the tool

Dynamics of the tool is required for the stability analysis and stability limit prediction. Tool dynamics can be measured using impact tests and modal analysis. However, considering many combinations of tool and tool holder even for one machine, this can be very time consuming approach especially for industrial environment. Two different cases will be considered for analytical modeling of the end mill dynamics. For slender end mills where the dynamics is mostly dominated by the tool modes, flexible tool-rigid holder model will be used. A general case will also be presented where the tool, tool holder and spindle dynamics are also included.

5.1. Flexible tool-rigid holder

Dynamic analysis is used to determine mode shapes and natural frequencies of the cutting tool structures. A modeling method for transverse vibrations of an end mill is developed. End mill is a segmented beam, one segment for the part with flute and the other segment for the shank. The beam model with two different geometric segments is shown in Fig. 9. $I1, I2$ and $A1$, $A2$ are the moment of inertias and the areas of the segments, respectively. $R(x)$ and $S(y)$ are the mode shapes, and $w1(x,t)$ and $w2(x,t)$ are the displacement functions. The governing equations of motion, neglecting the rotational inertia and shear formation, can be converted into the well-known Euler–Bernoulli equations:

$$EI1\frac{d^4R}{dx^4} - \rho A1\omega^2, \quad R = 0, 0 \leqslant x \leqslant L1,$$
$$EI2\frac{d^4S}{dy^4} - \rho A2\omega^2, \quad S = 0, 0 \leqslant y \leqslant L2, \tag{42}$$

where E is the modulus of elasticity and ρ is the density. The solution of Eq. (42) can be expressed as

$$R(x) = A1\cosh(\beta x) + A2\sinh(\beta x) + A3\cos(\beta x) + A4\sin(\beta x),$$
$$S(x) = A5\cosh(\alpha x) + A6\sinh(\alpha x) + A7\cos(\alpha x) + A8\sin(\alpha x), \tag{43}$$

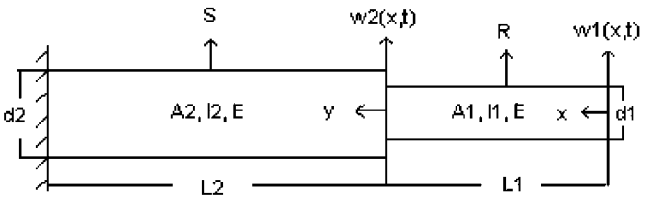

Fig. 9. The geometry of the beam with two different segments.

where $A1, A2, A3, A4, A5, A6, A7$ and $A8$ are arbitrary constants. It is necessary to accompany the general solutions with the boundary conditions. After applying the free boundary conditions at $x = 0$, i.e. bending moment and shear force must vanish; continuity equations at $x = L1$ and $y = 0$, i.e. displacement, slope, moment and shear force must be equal on both sides, and fixed boundary conditions $y = L2$, the following matrix equation is obtained [26]

$$[C]\{A\} = 0, \tag{44}$$

where A_j is the vector of the 8 arbitrary constants and the coefficient matrix $[C]$ is of dimension (8×8). These 8 conditions are sufficient to solve for the 8 arbitrary constants. The equations involving these constants are given in [26]. The characteristic equation is determined if $|C| = 0$. The natural frequencies are computed from the solution of characteristic equation as

$$\omega = (\beta L1)\sqrt{\frac{EI1}{\rho A1 L1^4}} \quad \text{or} \quad \omega = (\alpha L2)\sqrt{\frac{EI2}{\rho A2 L2^4}}. \tag{45}$$

The mode shapes according to the frequencies are obtained by combining $R(x)$ and $S(y)$ from Eq. (43).

5.2. Tool dynamics including machine flexibility

5.2.1. Receptance coupling substructure analysis for tool dynamics

In this model, the complete machine structure is divided into two parts: tool and tool holder/spindle. The description of the assembly model and the connection parameters are shown in Fig. 10 [24]. The four connection parameters (linear and torsional springs and dampers) must be determined to predict tool point frequency response function (FRF). According to these parameters, tool and tool holder/spindle FRFs are coupled using receptance coupling substructure analysis (RCSA). RCSA is a very efficient method for predicting dynamic response of tools without measurements for each tool, tool holder and spindle combination. The analytical model developed for the tool dynamics is used together with RCSA to determine the total dynamics of the machine.

In the formulation, the component modes are represented by H whereas G is for the assembly FRFs. Direct and cross deflection receptance terms (H_{11}, H_{22} and $H_{12} = -H_{21}$), displacement under applied force (L_{mn}), rotation under applied force (N_{mn}) and the rotation under applied moment (P_{mn}) for the component A are derived analytically [24,25]. For the calculations, density (ρ), elastic modulus (E), viscous damping coefficient (c) and second moment of inertia (I) are required. In the static analysis section, an analytic equation for the maximum displacement at the tool tip was derived which can be used to determine the stiffness of the tool. The effective diameter of the tool and the second moment of inertia can be calculated using the analytical equations presented in Part (1) of the paper [30] for segmented beam. The damping ratios for many HSS and carbide tools have been determined experimentally. Average values of $\zeta = 0.018$ and $\zeta = 0.012$ have been obtained from experimental data for HSS and carbide tools, respectively. These damping ratio values can then be used in the analysis of different tools.

For the tool holder/spindle component the direct deflection receptance term (H_{33}) is measured at the intersection location by impact test. L_{33}, N_{33} and P_{33} are assumed to be zero. Finally, after RCSA for the complete structure, the analytical displacement/force relationship at the tool tip (G_{11}), which is required for stability and chatter avoidance, is given by Schmizt et al. [25]:

$$\begin{aligned}
G_{11} &= \frac{X_1}{F_1} = H_{11} - H_{12}E_1^{-1}E_2 \\
&\quad - L_{12}E_3^{-1}\left(\left(k_qN_{21} + c_qN'_{21}\right) - E_4E_1^{-1}E_2\right), \\
E_1 &= \left(k_xH_{33} + k_xH_{22} + c_xH'_{33} + c_xH'_{22} + 1\right) \\
&\quad - E_3^{-1}E_4\left(k_xL_{33} + k_xL_{22} + c_xL'_{33} + c_xL'_{22}\right), \\
E_2 &= \left(k_xH_{21} + c_xH'_{21}\right) - E_3^{-1}\left(k_qN_{21} + c_qN'_{21}\right) \\
&\quad \times \left(k_xL_{33} + k_xL_{22} + c_xL'_{33} + c_xL'_{22}\right), \\
E_3 &= k_qP_{33} + k_qP_{22} + c_qP'_{33} + c_qP'_{22} + 1, \\
E_4 &= k_qN_{33} + k_qN_{22} + c_qN'_{33} + c_qN'_{22}, \\
H'_{mn} &= \mathrm{i}wH_{mn}, \quad L'_{mn} = \mathrm{i}wL_{mn}, \\
N'_{mn} &= \mathrm{i}wN_{mn}, \quad P'_{mn} = \mathrm{i}wP_{mn}.
\end{aligned} \tag{46}$$

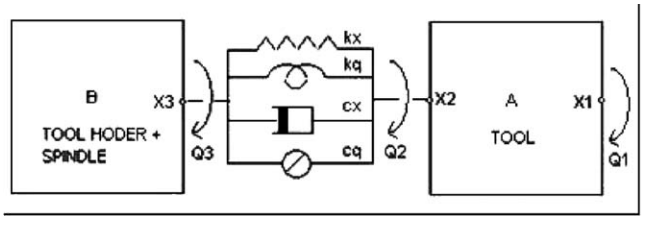

Fig. 10. Tool and tool holder/spindle assembly.

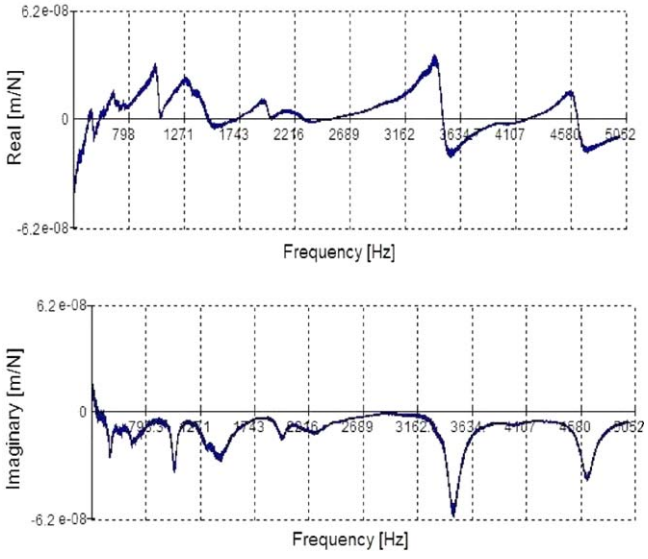

Fig. 11. Measured FRF at the tip of CAT40 tool holder/spindle combination.

Table 3
Stiffness and damping coefficients for the experiment

	$L/D = 8$ $L_{contact} = 36$	$L/D = 9$ $L_{contact} = 28$	$L/D = 10$ $L_{contact} = 20$	$L/D = 11$ $L_{contact} = 12$
k_x (N/m)	9.036×10^6	6.885×10^6	3.614×10^6	1.304×10^6
k_q (Nm/rad)	1.02×10^7	5.3×10^6	3.8×10^6	1.277×10^6
c_x (Ns/m)	445	368	228	141
c_q (Nms/rad)	54.17	71.44	78.09	79.34

5.2.2. Identification of interface parameters

In experiments, the tool point FRFs (G_{11}) of the tool/tool holder/spindle assembly are measured for different tools [26]. From the analytical component modes presented, and the experimental data the clamping stiffness and damping can be identified from tool point FRF. This is done using least squares error minimization method in order to minimize the overall error in the considered frequency range for the FRF.

5.3. Example application

A carbide end mill with 4 flutes, 8 mm diameter, and 100 mm length is used for test. Different lengths are selected for the measurement. The tool effective diameter and damping coefficient were determined as 7.49 mm and 5 Ns/m, respectively. The tool holder/spindle direct FRF (H_{33}) is measured at the free end in x/y directions is shown in Fig. 11. The same tool holder is used with different end mills, and therefore the same FRF (H_{33}) is used in RCSA. After the nonlinear least square evaluation, the stiffness and damping coefficients are determined as shown in Table 3. The measured and predicted FRFs using analytical component FRFs and RCSA are given for the shortest and longest tools Fig. 12. The agreement between the experimental results and the predictions is satisfactory.

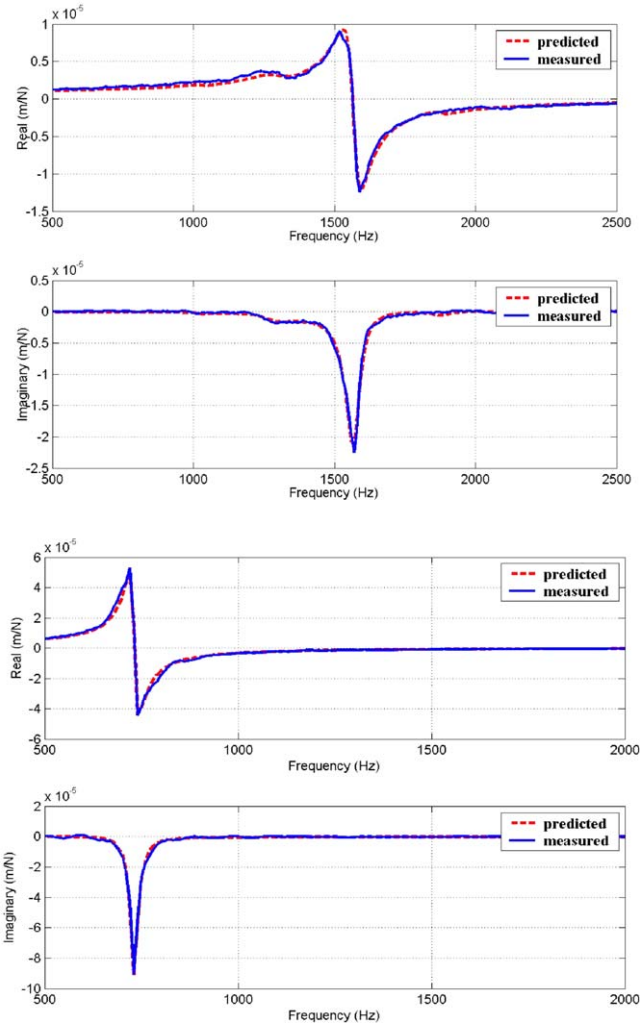

Fig. 12. Predicted and measured FRFs for $L/D = 8$ and $L/D = 11$.

6. Conclusions

Chatter is one of the major limitations in machining resulting in poor quality and low productivity. In this paper, analytical models which can be used to suppress chatter vibrations, and thus increase the performance in milling operations, are presented. Stability of milling is complicated due to the rotational cutting tool resulting in a time varying dynamics. The analytical milling stability model is based on the Fourier series expansion of the periodic terms and the Floquet's theorem. The method is very fast and practical in generating stability lobe diagrams which can be used to maximize chatter free material removal rate. This method is also extended to the analysis and design of variable pitch cutters which are effective in suppressing chatter in low cutting speeds as well. An analytical method is presented for modeling of end mill dynamics which eliminates the need for transfer function measurements for every tool assembly. The application of the models is demonstrated by several examples. These methods can be used in industrial processes for increased milling performance.

References

[1] J. Tlusty, M. Polacek, The stability of machine tools against self excited vibrations, ASME International Research in Production Engineering 1 (1963) 465–474.
[2] S.A. Tobias, Machine Tool Vibration, Blackie, London, 1969.
[3] F. Koenigsberger, J. Tlusty, Machine Tool Structures, Pergamon Press, Oxford, 1967.
[4] H. Opitz, F. Bernardi, Investigation and calculation of the chatter behavior of lathes and milling machines, Annals of the CIRP 18 (1) (1970) 335–343.

[5] R. Sridhar, R.E. Hohn, G.W. Long, General formulation of the milling process equation, Transactions of ASME, Journal of Engineering for Industry 90 (1968) 317–324.
[6] R. Sridhar, R.E. Hohn, G.W. Long, A stability algorithm for the milling process, Transactions of ASME, Journal of Engineering for Industry 90 (1968) 330–334.
[7] I. Minis, T. Yanushevsky, A new theoretical approach for the prediction of machine tool chatter in milling, Transactions of ASME, Journal of Engineering for Industry 115 (1993) 1–8.
[8] E. Budak, The mechanics and dynamics of milling thin-walled structures, Ph.D. Dissertation, University of British Columbia, 1994.
[9] Y. Altintas, E. Budak, Analytical prediction of stability lobes in milling, Annals of the CIRP 44 (1) (1995) 357–362.
[10] E. Budak, Y. Altintas, Analytical prediction of chatter stability in milling—part I: general formulation; part II: application to common milling systems, Transactions of ASME, Journal of Dynamic Systems, Measurement, and Control 120 (1998) 22–36.
[11] Y. Altintas, E. Shamoto, P. Lee, E. Budak, Analytical prediction of stability lobes in ball-end-milling, Transactions of ASME, Journal of Manufacturing Science and Engineering 121 (1999) 586–592.
[12] Y. Altintas, Analytical prediction of three dimensional chatter stability in milling, Japan Society of Mechanical Engineers, International Journal Series: Mechanical Systems, Machine Elements and Manufacturing 44 (3) (2001) 717–723.
[13] M.A. Davies, B. Dutterer, J.R. Pratt, T.J. Burns, The stability of low radial immersion milling, Annals of the CIRP 49 (1) (2000) 37–40.
[14] W.T. Corpus, W.J. Endres, Added stability lobes in machining processes that exhibit periodic time variation, Transactions of ASME, Journal of Manufacturing Science and Engineering 126 (2004) 467–474.
[15] T. Insperger, B.P. Mann, G. Stepan, P.V. Bayly, Stability of upmilling and down-milling, part 1; alternative analytical methods, International Journal of Machine Tools and Manufacture 43 (1) (2003) 25–34.
[16] S.D. Merdol, Y. Altintas, Multi frequency solution of chatter stability limits for low immersion milling, Transactions of ASME Journal of Manufacturing Science and Engineering 126 (2004) 459–466.
[17] J. Slavicek, The effect of irregular tooth pitch on stability of milling, in: Proceedings of the Sixth MTDR Conference, Pergamon Press, London, 1965, pp. 15–22.
[18] H. Opitz, E.U. Dregger, H. Roese, Improvement of the dynamic stability of the milling process by irregular tooth pitch, in: Proceedings of the Advanced MTDR Conference, vol. 7, 1966, pp. 213–227.
[19] P. Vanherck, Increasing milling machine productivity by use of cutters with non-constant cutting edge pitch. in: Proceedings of the Eigth MTDR Conference, Manchester, 1967, pp. 947–960.
[20] J. Tlusty, F. Ismail, W. Zaton, Use of special milling cutters against chatter, NAMRC 11, University of Wisconsin, SME, 1983, pp. 408–415.
[21] Y. Altintas, S. Engin, E. Budak, Analytical stability prediction and design of variable pitch cutters, Transactions of ASME, Journal of Manufacturing Science and Engineering 121 (1999) 173–178.
[22] E. Budak, An analytical design method for milling cutters with non-constant pitch to increase stability—Part I: theory. Part II: application, Transactions of ASME, Journal of Manufacturing Science and Engineering 125 (2003) 29–38.
[23] Y. Altintas, Manufacturing Automation, Cambridge University Press, Cambridge, 2000.
[24] T.L. Schmitz, Predicting high speed machining dynamics by substructure analysis, Annals of the CIRP 49 (1) (2000) 303–308.
[25] T.L. Schmitz, M.A. Davies, M.D. Kennedy, Tool point frequency response prediction for high speed machining by RCSA, Transactions of ASME, Journal of Manufacturing Science and Engineering 123 (2001) 700–707.
[26] E. Kivanc, E. Budak, Structural modeling of end mills for form error and stability analysis, International Journal of Machine Tools and Manufacture 44 (11) (2004) 1151–1161.
[27] M. Weck, Y. Altintas, C. Beer, CAD assisted chatter free NC tool path generation in milling, International Journal of Machine Tools and Manufacture 34 (1994) 879–891.
[28] A. Tekeli, E. Budak, Maximization of chatter-free material removal rate in end milling using analytical methods, Machining Science & Technology 9 (2) (2005) 47–167.
[29] E. Budak, A. Tekeli, Maximizing chatter free material removal rate in milling through optimal selection of axial and radial depth of cut pairs, Annals of the CIRP 54 (1) (2005) 353–356.
[30] E. Budak, Analytical models for high performance milling, part I: cutting forces, deflections and tolerance integrity, International Journal of Machine Tools and Manufacture, doi:10.1016/j.machtools.2005.09.009.